Supporting Information

Contents

Figure S8. RSBI analysis of complex **2** with the inclusion of empirical dispersion. (a) AIM bond paths motif, (b) NCI *iso*-surface at s(r) = 0.5, (c) ELI-D localization domain representation at *iso*-value of 1.3, (d) ELI-D distribution mapped on a Si-Si ELI-D basin.

Figure S9. NCI *iso*-surface at s(**r**) = 0.5 of **2**. Side view.

Table S2. Topological and integrated bond properties from AIM and ELI-D. Values derived from the inclusion of empirical dispersion are given in italics.

Table S3. AIM atomic and fragmental charges (in e) of **1** and **2**. Values derived from the inclusion of empirical dispersion are given in italics.

4. Additional References

1. Experimental Section

General. Reagents were obtained commercially and were used as received. Dry acetonitrile, dichloromethane, *n*-hexane and toluene were collected from a SPS800 mBraun solvent system and stored over 4 Å molecular sieves. Diethylether was dried over sodium/benzophenone by refluxing under argon atmosphere. Deuterated solvents and 1,2-difluorobenzene were degassed by argon and stored over 4 Å molecular sieves. 5-bromo-6-diphenylphosphino-acenaphthene[S1] and (5-diphenylphosphinoacenaphth-6-yl)chlorodimethylsilane[S2] was prepared according to literature procedures. ^{1}H-, ^{13}C-, ^{29}Si- and ^{31}P-NMR spectra were recorded at r.t. using a Bruker Avance 600 MHz spectrometer and are referenced to tetra-methylsilane (^{1}H, ^{13}C, ^{29}Si) and phosphoric acid (85% in water) (^{31}P). Chemical shifts are reported in parts per million (ppm) and coupling constants (*J*) are given in Hertz (Hz). Electron impact mass spectroscopy (HREIMS) was carried out using a Finnigan MAT 95. The ESI HRMS spectra were obtained with a Bruker Impact II spectrometer. Dichloromethane/acetonitrile or acetonitrile solutions ($c = 1 \cdot 10^{-6}$ mol l^{-1}) were injected directly into the spectrometer at a flow rate of 3 µl min^{-1}. Nitrogen was used both as a drying gas and for nebulization with flow rates of approximately 5 l min^{-1} and a pressure of 5 psi, respectively. Pressure in the mass analyzer region was usually about $1 \cdot 10^{-5}$ mbar. Spectra were collected for one minute and averaged. The nozzle-skimmer voltage was adjusted individually for each measurement.

Synthesis of Bis(5-diphenylphosphinoacenaphth-6-yl)tetramethyldisilane (1). Method A. To a solution of 5-bromo-6-diphenylphosphinoacenaphthene (5.00 g, 12.0 mmol, 2.00 eq.) and toluene (50 mL), *n*-butyllithium (12.0 mmol, 2.5 M in *n*-hexane, 2.00 eq.) were added at room temperature and stirred for 1 h.[S3] After a yellowish suspension is formed dichlorotetramethyldisilane (1.12 g, 6.00 mmol, 1.00 eq.) was added and the reaction mixture stirred for 1h. Volatile parts were removed under reduced pressure and dichloromethane (50 mL) was added to the residue. After aqueous workup the solvent was removed by rotary evaporation and the light brown residue was washed with *n*-hexane and diethylether. The pale yellow residue was recrystallized by dichloromethane/*n*-hexane yielding **1** as colourless crystals (2.31 g, 2.92 mmol, 49%, T(decomp.) 235°C). **Method B.** To a greenish solution of 4,4'-di-*tert*-butylbiphenyl (31.9 mg, 0.12 mmol, 0.20 eq.) and lithium (9.2 mg, 1.32 mmol, 2.20 eq.) in tetrahydrofuran (20 mL), a solution of (5-diphenylphosphinoacenaphth-6-yl)chlorodimethylsilane (520 mg, 1.20 mmol, 2.00 eq.) in tetrahydrofuran (20 mL) was added at 0°C dropwise until the solution turned red. After 30 minutes the solution turned green again and the solution containing (5-diphenylphosphinoacenaphth-6-yl)chlorodimethylsilane was added dropwise until it turned red again. That procedure was repeated until the whole solution of (5-diphenylphosphinoacenaphth-6-yl)chlorodimethylsilane was added. After the colour turned green, the solvent was removed, the brownish residue was dissolved in dichloromethane and the precipitate was separated from the solution by filtration. After aqueous workup the solution was layered with *n*-hexane yielding **1** as colourless crystals (0.43 g, 0.54 mmol, 90%, T(decomp.) 235°C).

^{1}H NMR (601 MHz, C_6D_6): δ [ppm] = 8.09 (dd, $^{3}J(^{1}H\text{-}^{1}H)$ = 7.3 Hz, $^{3}J(^{31}P\text{-}^{1}H)$ = 2.4 Hz, 2H, H-4), 7.64 (m, 2H, H-7), 7.23 (m, 8H, H-*m*), 6.98 (d, $^{3}J(^{1}H\text{-}^{1}H)$ = 7.6 Hz, 2H, H-8), 6.95 (m, 14H, H-3, H-*o*, H-*p*), 3.40 (m, 4H, H-2), 2.96 (m, 8H, H-1, H-2), 0.78 (jjs, 12H, $SiCH_3$). **^{13}C{^{1}H} NMR (151 MHz, C_6D_6):** δ [ppm] = 150.2 (s, qC, C-2a), 147.6 (s, qC, C-8a) , 142.3

(d, $^{2}J(^{31}P\text{-}^{13}C)$ = 34.7 Hz, qC, C-5a), 140.7 (s, CH, C-4), 140.4 (s, qC, C-8b), 140.3 (d, $J(^{31}P\text{-}^{13}C)$ = 9.7 Hz, qC, C-5), 140.0 (s, CH, C_7), 136.6 (m, qC, C-6), 133.1 (d, $^{2}J(^{31}P\text{-}^{13}C)$ = 15.9 Hz, CH, C-*o*), 130.2 (s, CH, C-*m*, C-*i*), 130.1 (s, CH, C-*m* or C-*i*), 128.3 (s, CH, C-*p*), 127.7 (s, CH, C-*p*), 119.8 (m, CH, C-3, C_8), 119.3 (s, CH, C_8), 30.3(s, CH_2, C-2), 29.9j (s, CH_2, C-1), 5.2 (dd, $J(^{31}P\text{-}^{13}C)$ = 15.0 Hz, $^{3}J(^{31}P\text{-}^{13}C)$ = 5.9 Hz, $SiCH_3$). **^{29}Si{^{1}H} NMR (119 MHz, C_6D_6):** δ [ppm] = –20.1 (dd, $J(^{31}P\text{-}^{29}Si)$ = 25.7 Hz, $J(^{31}P\text{-}^{29}Si)$ = 5.1 Hz). **^{31}P{^{1}H} NMR (243 MHz, C_6D_6):** δ [ppm] = –16.3 (s). **HRESIMS:** calcd for $C_{52}H_{48}NaP_2Si_2$ $[M+Na]^+$, 813.26620; found, 813.26531.

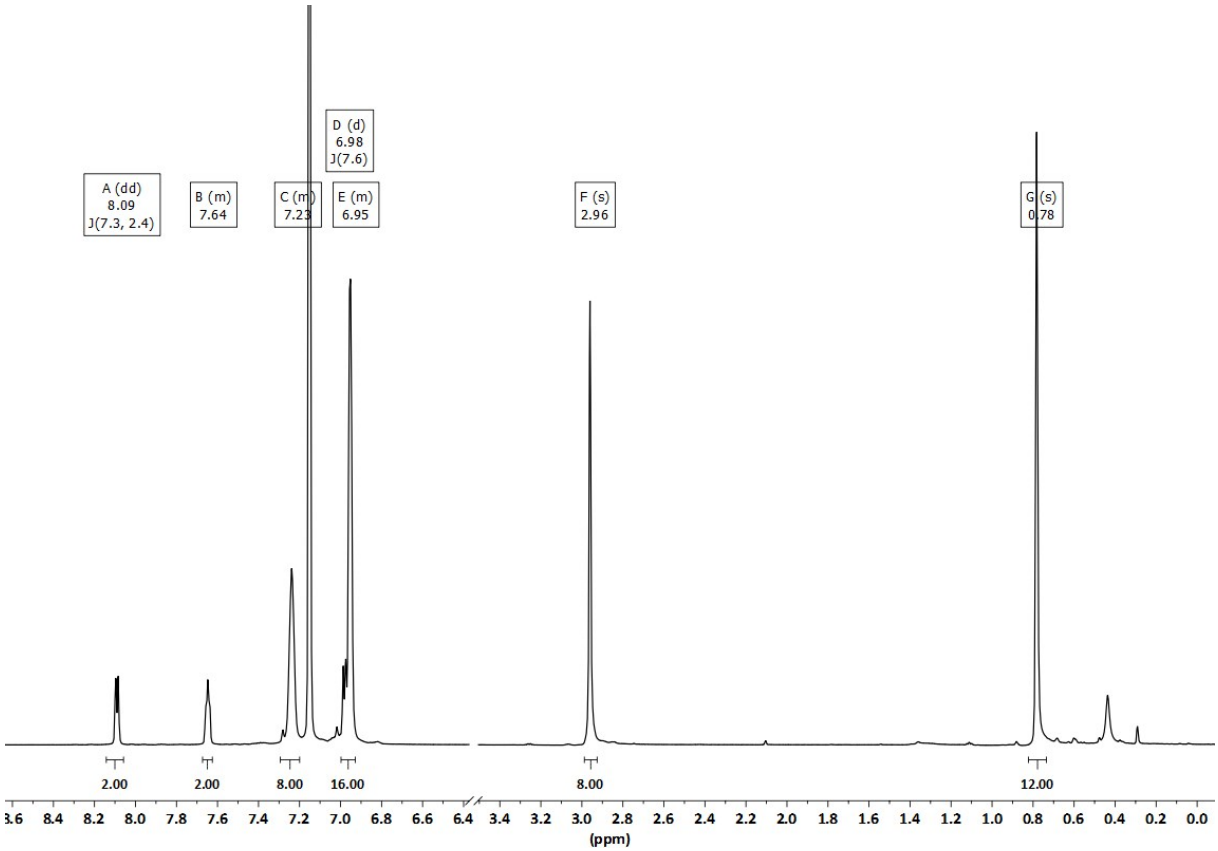

Figure 1a. ^{1}H-NMR spectrum (C_6D_6) of **1**.

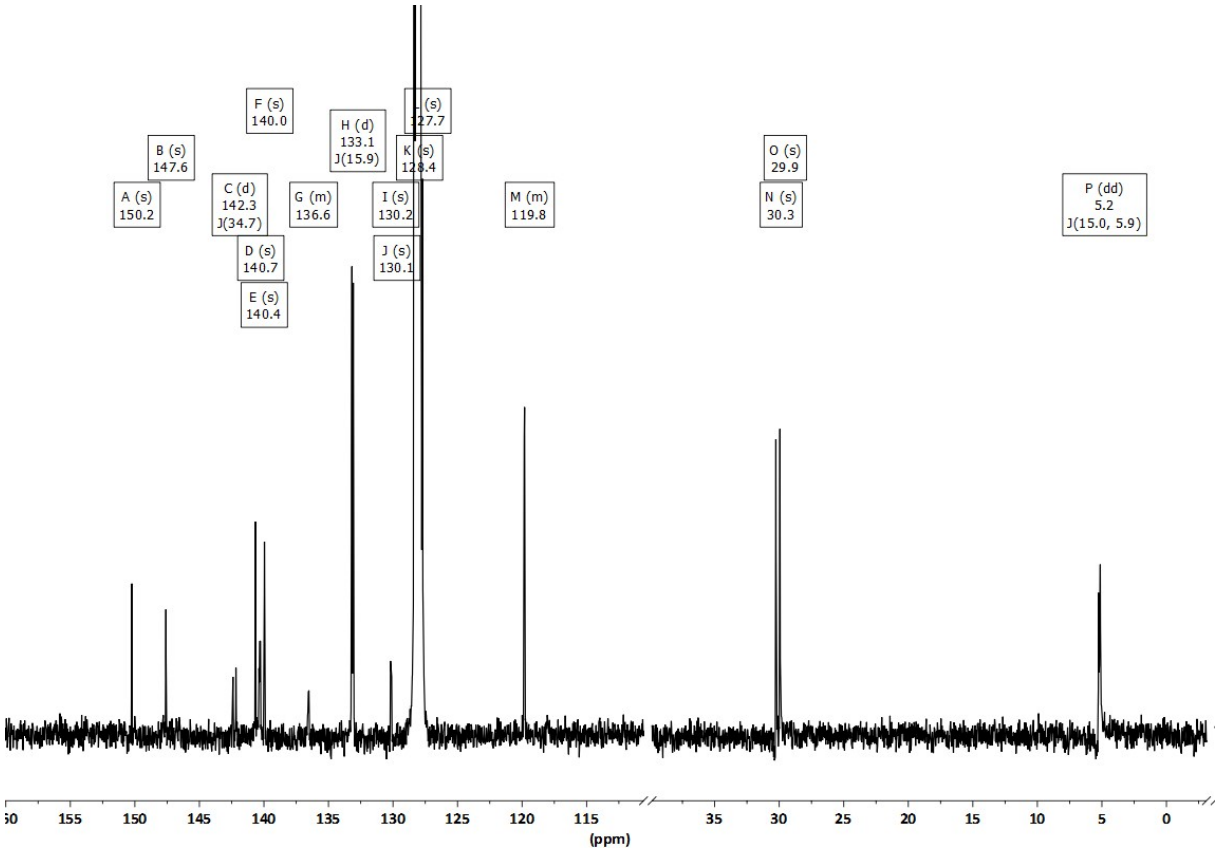

Figure 1b. $^{13}C\{^{1}H\}$-NMR spectrum (C_6D_6) of **1**.

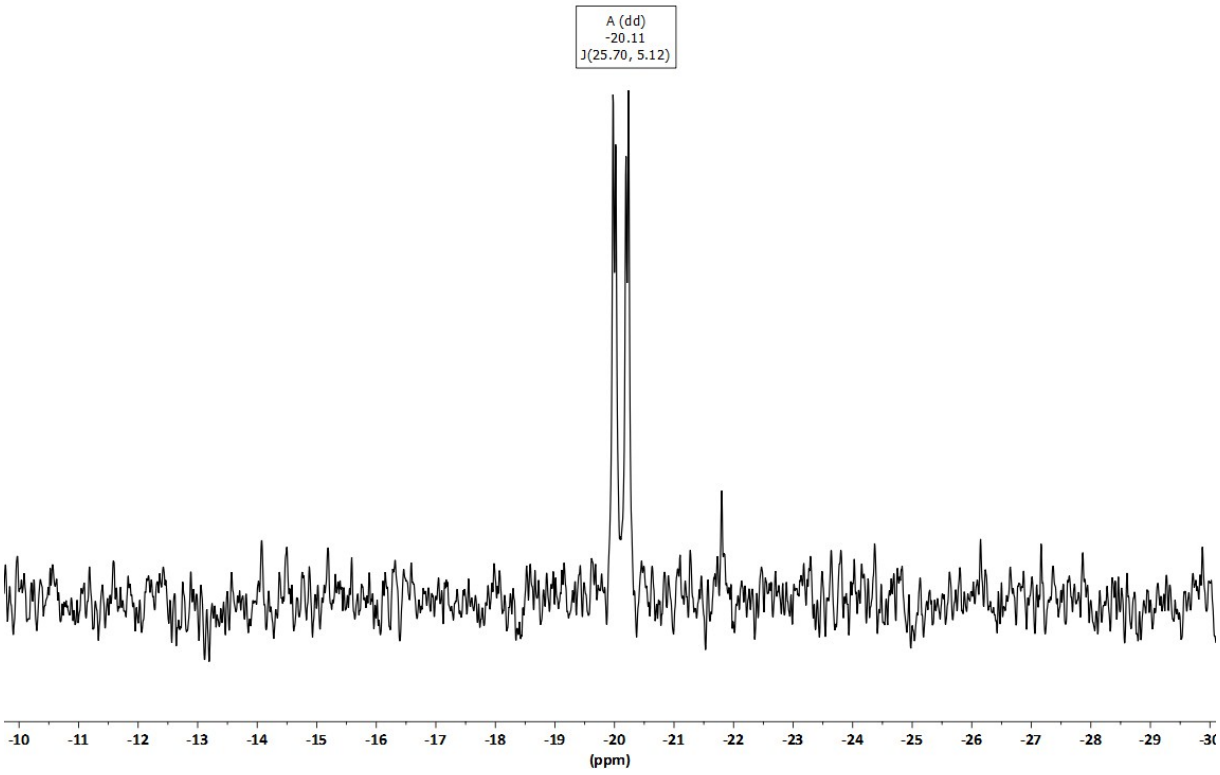

Figure 1c. $^{29}Si\{^{1}H\}$-NMR spectrum (C_6D_6) of **1**.

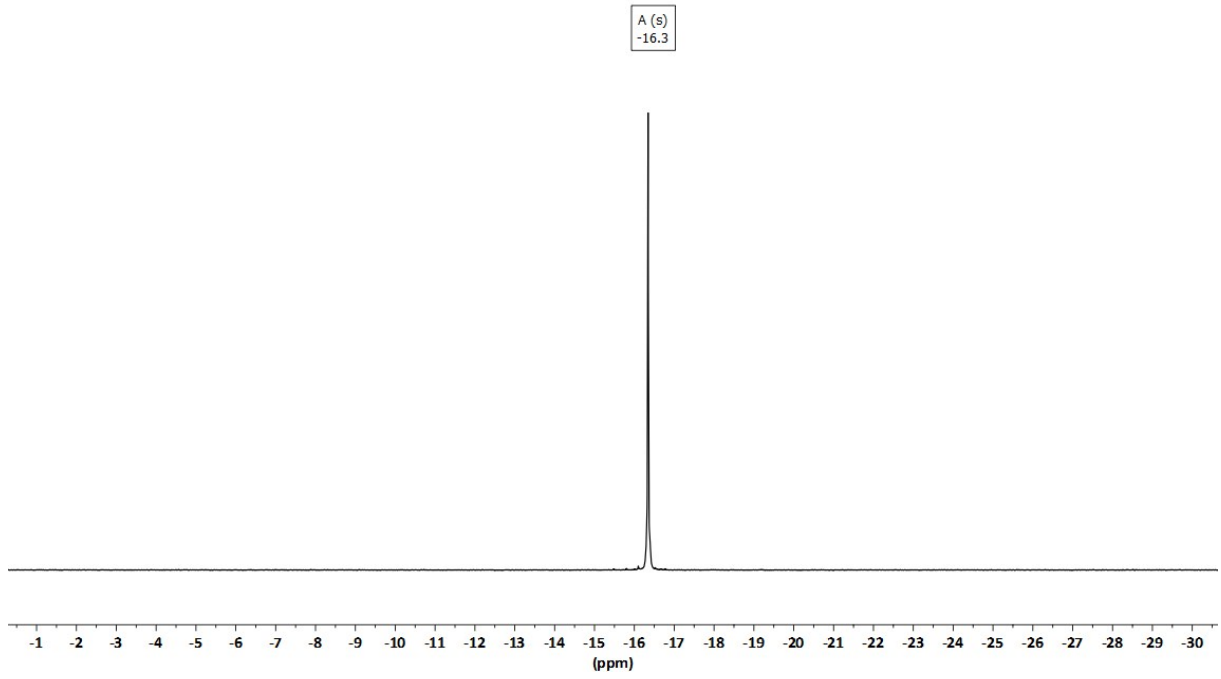

Figure 1d. $^{31}P\{^{1}H\}$-NMR spectrum (C_6D_6) of **1**.

Synthesis of Bis((5-diphenylphosphinoacenaphth-6-yl)dimethylsilyl)rhodium(III) chloride (2). Bis(5-diphenylphosphinoacenaphth-6-yl)tetramethyldisilane (**1**) (200 mg, 0.25 mmol, 1.00 eq.) and chlorobis(ethylene)rhodium dimer (49.2 mg, 0.13 mmol, 0.50 eq.) were dissolved in 1,2-difluorobenzene (10 mL) and the reaction mixture was stirred for 2 d. The solvent was removed under reduced pressure and the brownish residue was washed with *n*-hexane. The residue was dissolved in 1,2-difluorobenzene and the precipitate was separated from the solution by filtration. The solution was layered with *n*-hexane affording **2** as yellowish crystals (167 mg, 0.17 mmol, 68%, T(decomp.) 260°C).

^{1}H NMR (601 MHz, C_6D_6): δ [ppm] = 8.13 (m, 8H, H-*m*), 7.67 (d, $^{3}J(^{1}H\text{-}^{1}H)$ = 7.1 Hz, 2H, H-7), 7.58 (dt, $^{3}J(^{1}H\text{-}^{1}H)$ = 7.1 Hz, $^{3}J(^{31}P\text{-}^{1}H)$ = 5.5 Hz, 2H, H-4), 7.18 (d, $^{3}J(^{1}H\text{-}^{1}H)$ = 7.5 Hz, 4H, H-*o*), 7.07 (t, $^{3}J(^{1}H\text{-}^{1}H)$ = 7.4 Hz, 2H, H-*p*) 7.03 (d, $^{3}J(^{1}H\text{-}^{1}H)$ = 7.0 Hz, 2H, H-8), 6.94 (m, 6H, H-*o*), 6.91 (d, $^{3}J(^{1}H\text{-}^{1}H)$ = 7.3 Hz, 2H, H-3), 2.90 (m, 4H, H-1), 2.87 (m, 4H, H-2), 0.37 (s, 6H, $SiCH_3$), 0.19 (s, 6H, $SiCH_3$). **^{13}C{^{1}H} NMR (151 MHz, C_6D_6):** δ [ppm] = 151.2 (s, qC, C-2a), 147.3 (s, qC, C-8a), 140.2 (t, $^{2}J(^{31}P\text{-}^{13}C)$ = 7.8 Hz, qC, C-5a), 139.2 (t, $^{2}J(^{31}P\text{-}^{13}C)$ = 4.1 Hz, qC, C-5), 137.3 (s, CH, C-4), 136.5 (t, $J(^{31}P\text{-}^{13}C)$ = 7.3 Hz, qC, C-6), 135.2 (dt, $J(^{103}Rh\text{-}^{13}C)$ = 11.2 Hz, $^{3}J(^{31}P\text{-}^{13}C)$ = 5.4 Hz, CH, C-*m*), 134.6 (s, CH, C-7), 134.0 (t, $J(^{31}P\text{-}^{13}C)$ = 23.2 Hz, qC, C-*i*), 129.5 (d, $^{2}J(^{31}P\text{-}^{13}C)$ = 21.7 Hz, qC, C-*o*), 128.0 (s, CH, C-*p*), 122.1 (m, qC, C-8b), 120.1 (s, CH, C_8), 30.1(s, CH_2, C-2), 118.8 (t, $^{3}J(^{31}P\text{-}^{13}C)$ = 4.2 Hz, qC, C-3), 29.9 (s, CH_2, C-2), 29.8 (s, CH_2, C-1), 9.6 (s, $SiCH_3$), 7.5 (s, $SiCH_3$). **^{29}Si{^{1}H} NMR (119 MHz, C_6D_6):** δ [ppm] = 23.7 (dt, $J(^{103}Rh\text{-}^{29}Si)$ = 29.6 Hz, $J(^{31}P\text{-}^{29}Si)$ = 13.4 Hz). **^{31}P{^{1}H} NMR (243 MHz, C_6D_6):** δ [ppm] = 20.2 (d, $J(^{103}Rh\text{-}^{31}P)$ = 112.6 Hz). **HRESIMS:** calcd for $C_{52}H_{48}P_2RhSi_2$ $[M\text{-}Cl]^+$, 893.18193; found, 893.18049.

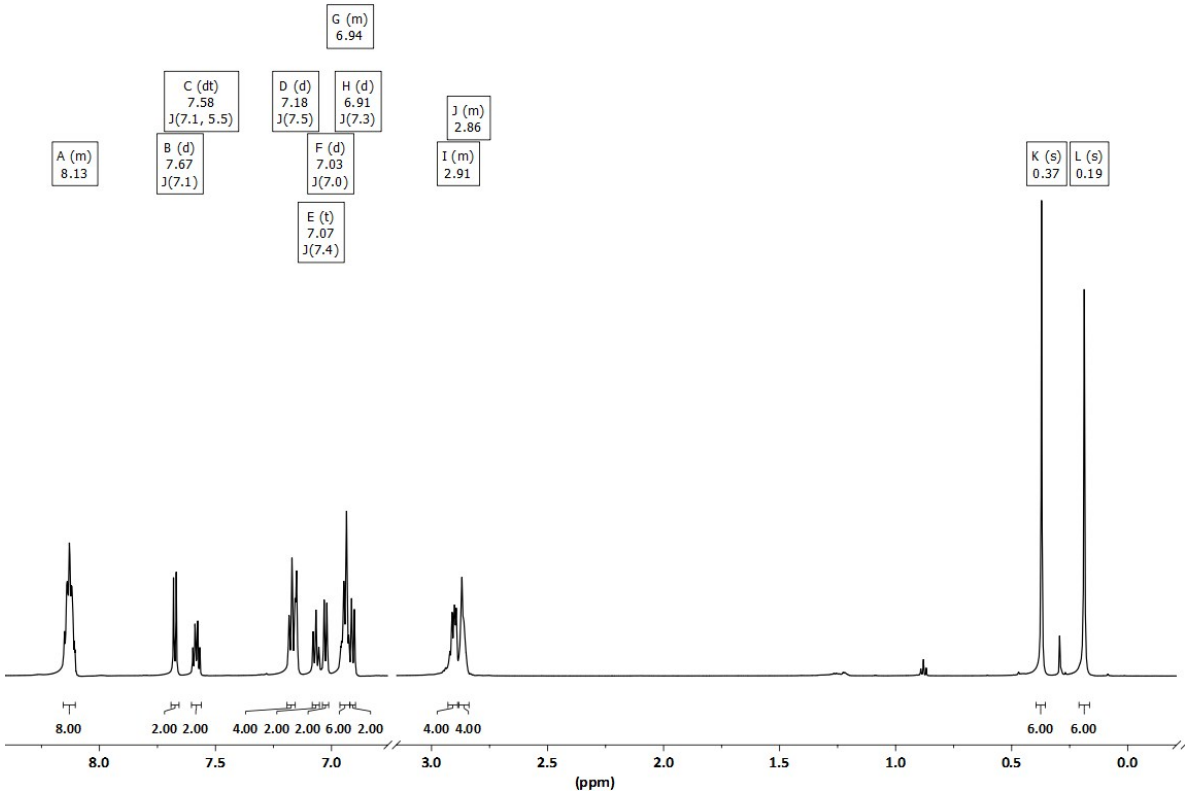

Figure 2a. ^{1}H-NMR spectrum (C_6D_6) of **2**.

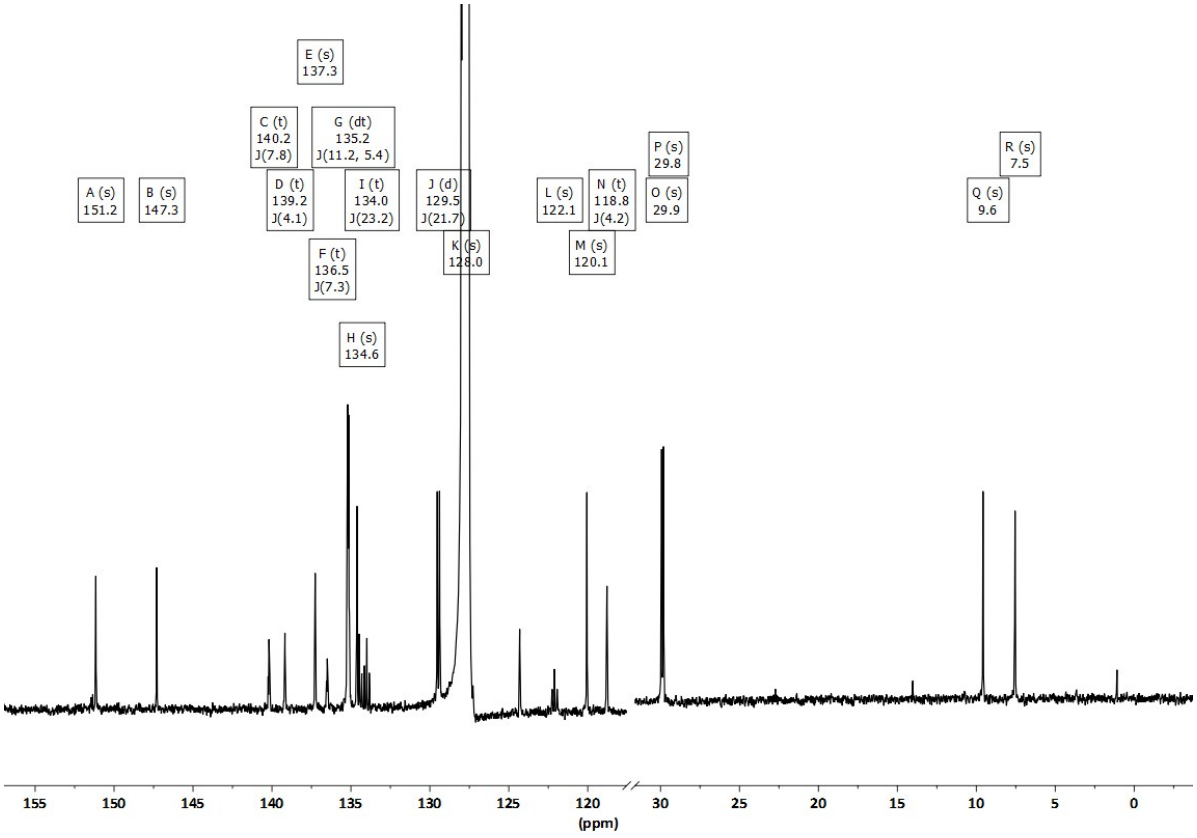

Figure 2b. ^{13}C{^{1}H}-NMR spectrum (C_6D_6) of **2**.

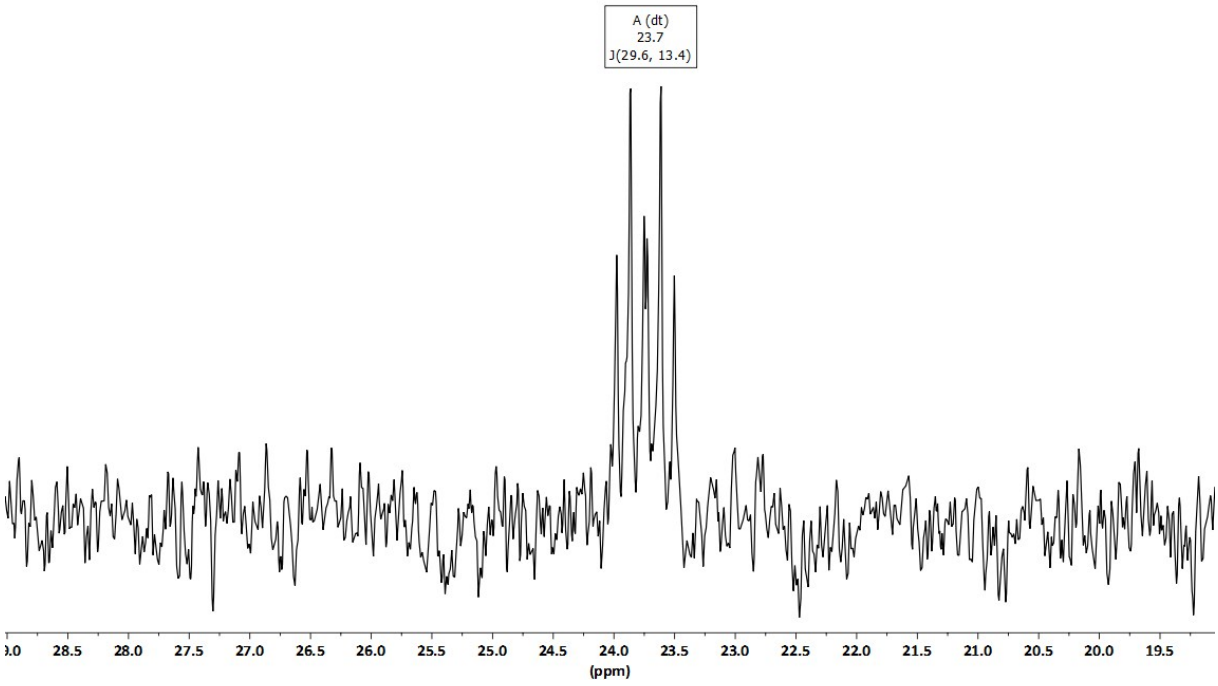

Figure 2c. $^{29}Si\{^{1}H\}$-NMR spectrum of spectrum (C_6D_6) of **2**.

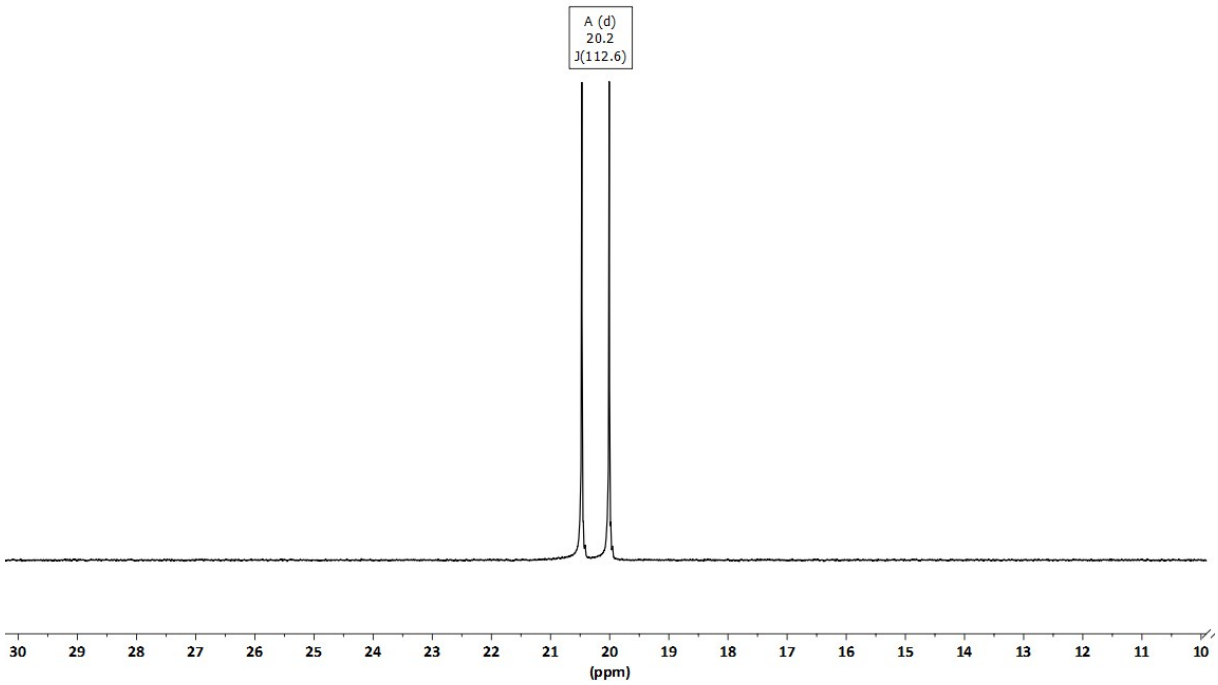

Figure 2d. $^{31}P\{^{1}H\}$-NMR spectrum of spectrum (C_6D_6) of **2**.

Synthesis of 1,1,2,2-tetramethyl-1,2-diphenyldisilane. To a greenish solution of 4,4'-di-*tert*-butylbiphenyl (0.47 g, 1.76 mmol, 0.20 eq.) and lithium (0.13 g, 19.3 mmol, 2.20 eq.) in tetrahydrofuran (20 mL), a solution of dimethylphenylchlorosilane (3.00 g, 17.6 mmol, 2.00 eq.) in tetrahydrofuran (20 mL) was added at room temperature dropwise until the solution turned red. After 30 minutes the solution turned green again and the solution containing dimethylphenylchlorosilane was added dropwise until it turned red again. That procedure was repeated until the whole solution of dimethylphenylchlorosilane was added. The solvent was removed and the slightly yellowish oil was distilled at 110°C to obtain 1,1,2,2-tetramethyl-1,2-diphenyldisilan as a colorless oil (2.02 g, 7.46 mmol, 85%). The measured NMR chemical shifts agree with the literature.[S4]

^{1}H NMR (601 MHz, $CDCl_3$): δ [ppm] = 7.55 (m, 4H), 7.37 (m, 6H), 0.36 (s, 12H). **^{13}C{^{1}H} NMR (151 MHz, $CDCl_3$):** δ [ppm] = 137.6 (s), 134.1 (s), 129.3 (s), 128.0 (s), –3.6 (s). **^{29}Si{^{1}H} NMR (119 MHz, $CDCl_3$):** δ [ppm] = –17.1 (s).

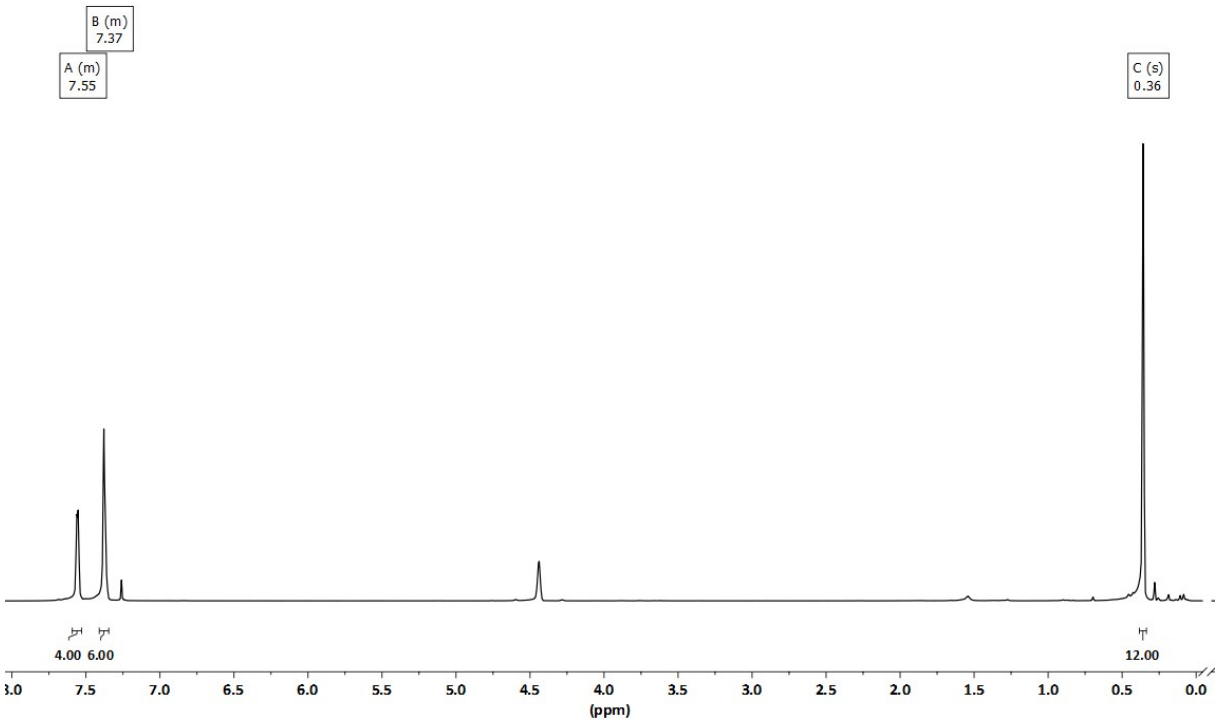

Figure 3a. ^{1}H-NMR spectrum of 1,1,2,2-tetramethyl-1,2-diphenyldisilane ($CDCl_3$).

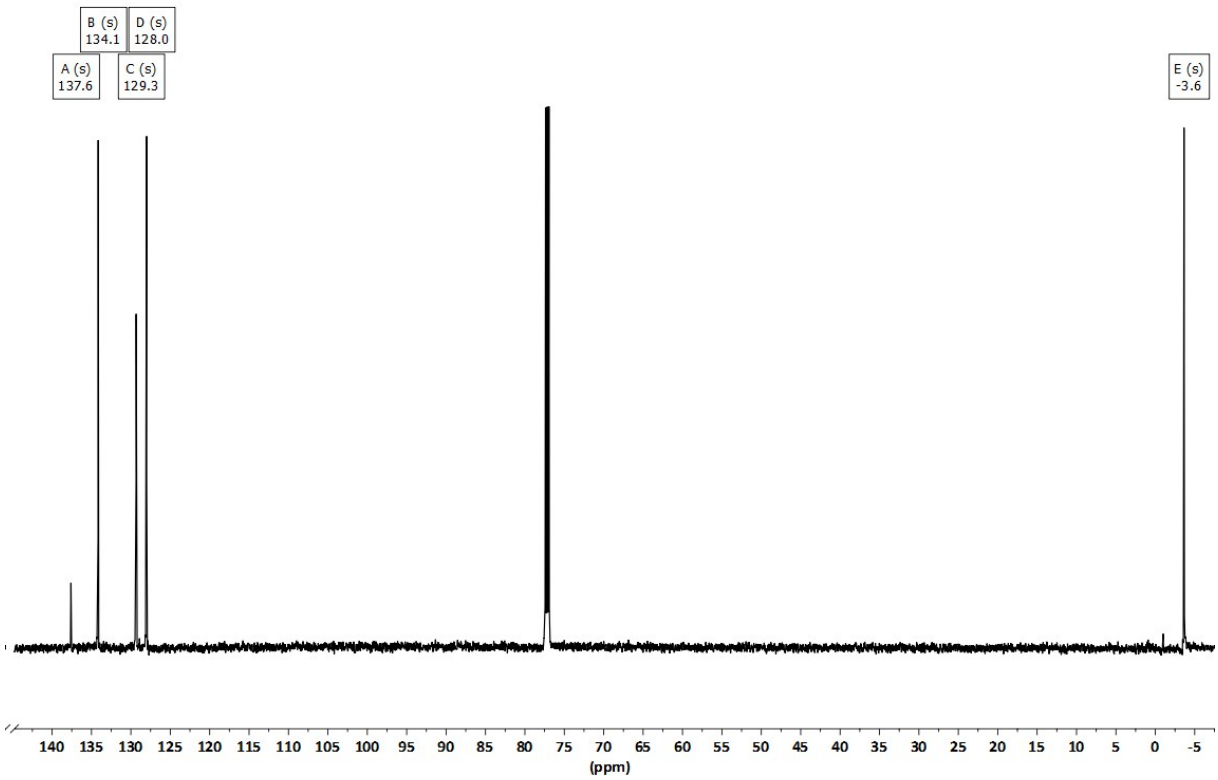

Figure 3b. ^{13}C{^{1}H}-NMR spectrum of 1,1,2,2-tetramethyl-1,2-diphenyldisilane ($CDCl_3$).

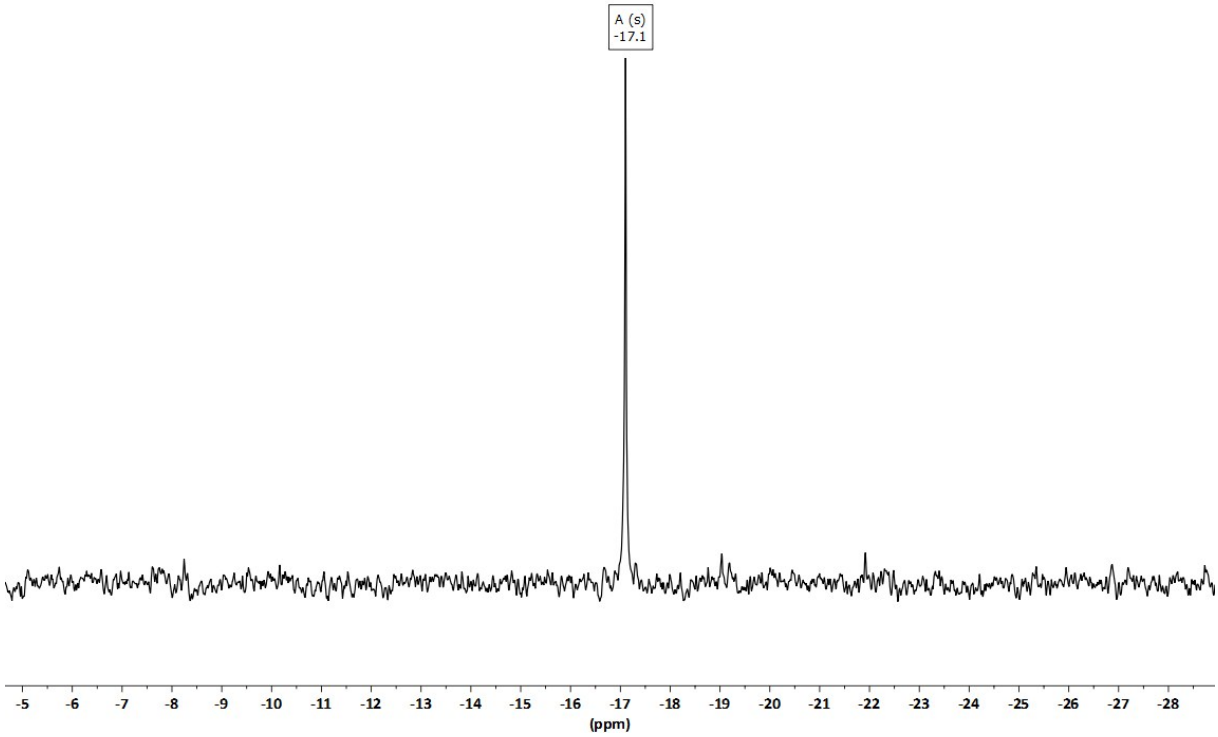

Figure 3c. $^{29}Si\{^{1}H\}$-NMR spectrum of 1,1,2,2-tetramethyl-1,2-diphenyldisilane ($CDCl_3$).

Synthesis of hexaphenyldisilane. To a greenish solution of 4,4'-di-*tert*-butylbiphenyl (0.36 g, 1.36 mmol, 0.20 eq.) and lithium (0.10 g, 15.0 mmol, 2.20 eq.) in tetrahydrofuran (20 mL), a solution of triphenylchlorosilane (4.00 g, 13.6 mmol, 2.00 eq.) in tetrahydrofuran (20 mL) was added at room temperature dropwise until the solution turned red and a colorless solid is formed. After 30 minutes the suspension turned green again and the solution containing triphenylchlorosilane was added dropwise until it turned red again. That procedure was repeated until the whole solution of triphenylchlorosilane was added. The solvent was decanted, the colorless solid washed with *n*-hexane and dried *in vacuo* to obtain hexaphenyl-disilane (3.36 g, 6.48 mmol, 95%). The measured nmr chemical shifts agree with the literature.[S4]

^{1}H NMR (601 MHz, $CDCl_3$): δ [ppm] = 7.35 (m, 6H), 7.24 (m, 24H). **^{13}C{^{1}H} NMR (151 MHz, $CDCl_3$):** δ [ppm] = 136.6 (s), 134.8 (s), 129.4 (s), 128.0 (s). **^{29}Si{^{1}H} NMR (119 MHz, $CDCl_3$):** δ [ppm] = –24.5 (s).

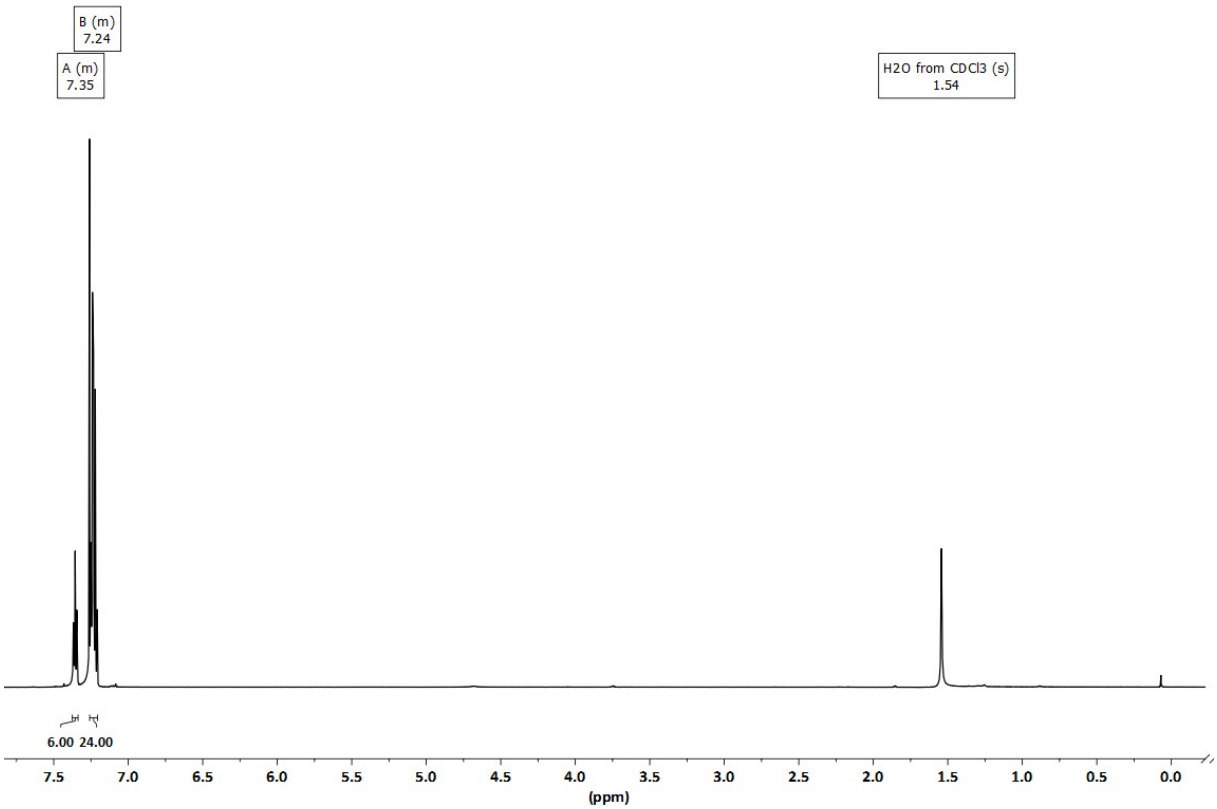

Figure 4a. ^{1}H-NMR spectrum of hexaphenyldisilane ($CDCl_3$).

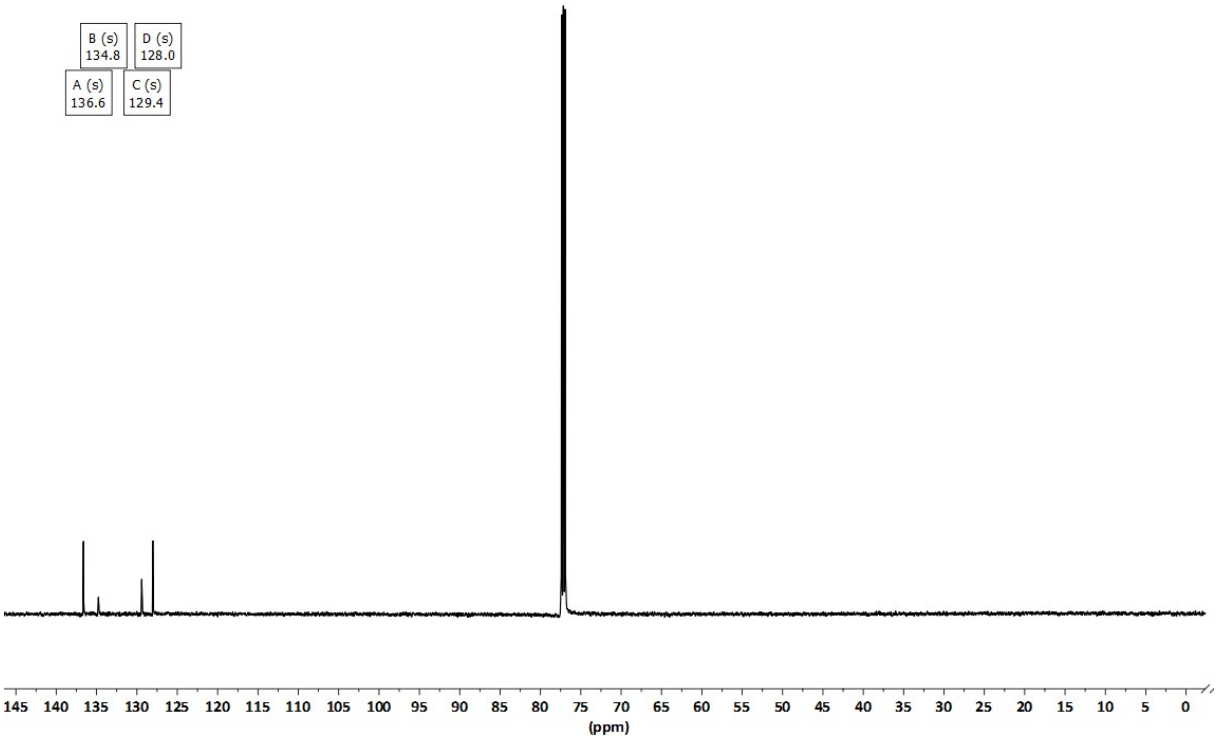

Figure 4b. ^{13}C{^{1}H}-NMR spectrum of hexaphenyldisilane ($CDCl_3$).

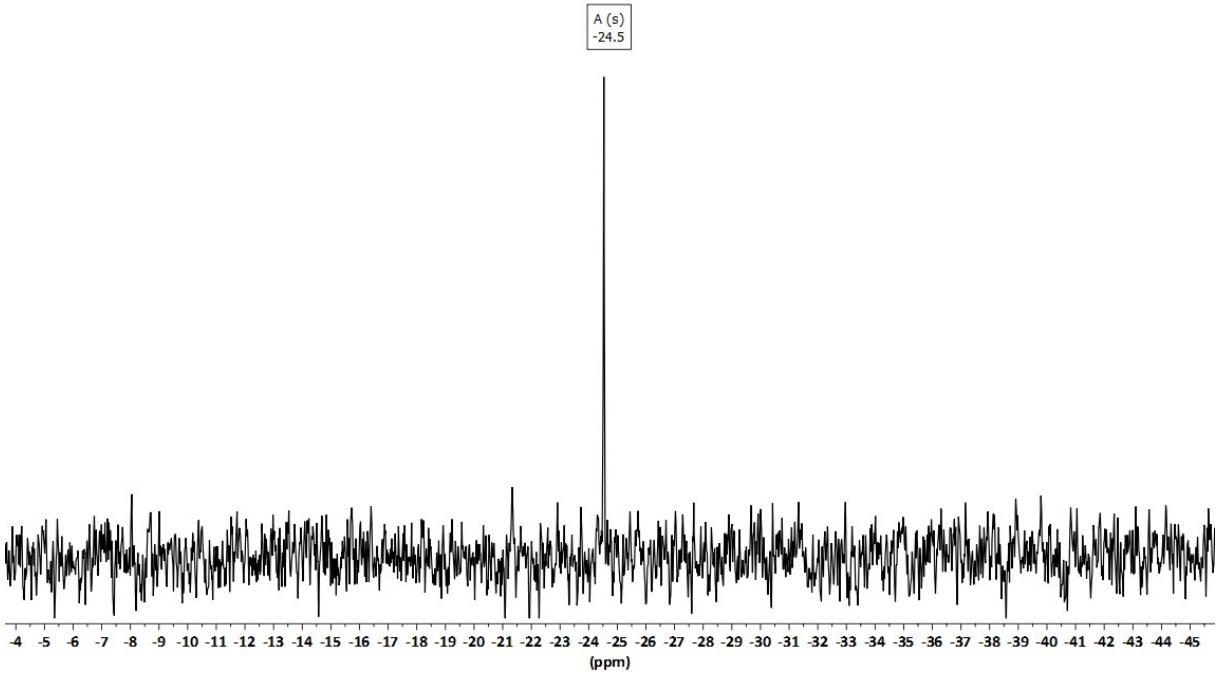

Figure 4c. $^{29}Si\{^{1}H\}$-NMR spectrum of hexaphenyldisilane ($CDCl_3$).

2. Crystallography

Intensity data of **1** and **2** was collected on a Bruker Venture D8 diffractometer at 100 K with graphite-monochromated Mo-Kα (0.7107 Å) radiation. All structures were solved by direct methods and refined based on F^2 by use of the SHELX program package as implemented in WinGX.[S5,S6] All non-hydrogen atoms were refined using anisotropic displacement parameters. Hydrogen atoms attached to carbon atoms were included in geometrically calculated positions using a riding model. Crystal and refinement data are collected in Table S1. Figures were created using DIAMOND.[S7] Crystallographic data for the structural analyses have been deposited with the Cambridge Crystallographic Data Centre. Copies of this information may be obtained free of charge from The Director, CCDC, 12 Union Road, Cambridge CB2 1EZ, UK (Fax: +44-1223-336033; e-mail: deposit@ccdc.cam.ac.uk or http://www.ccdc.cam.ac.uk).

Table S1. Crystal data and structure refinement of **1** and **2**.

	1	**2**·1/2 $F_2C_6H_4$
Formula	$C_{52}H_{48}P_2Si_2$	$C_{55}H_{50}ClFP_2RhSi_2$
Formula weight, g mol^{-1}	791.02	986.43
Crystal system	Monoclinic	Orthorhombic
Crystal size, mm	0.06 × 0.05 × 0.05	0.08 × 0.06 × 0.05
Space group	$P2_1/c$	Pcca
a, Å	17.918(5)	44.7754(14)
b, Å	13.341(5)	11.8417(4)
c, Å	19.445(5)	16.7861(5)
α, º	90	90
β, º	117.054(5)	90
γ, º	90	90
V, Å^3	4140(2)	8900.3(5)
Z	4	8
ρ_{calcd}, Mg m^{-3}	0.200	0.613
μ (Mo $K\alpha$), mm^{-1}	1.269	1.472
F(000)	1672	4072
θ range, deg	2.35 to 30.09	2.50 to 36.35
Index ranges	–25 ≤ h ≤ 25	–74 ≤ h ≤ 74
	–18 ≤ k ≤ 18	–19 ≤ k ≤ 19
	–27 ≤ l ≤ 27	–28 ≤ l ≤ 27
No. of reflns collected	415591	241985
Completeness to θ_{max}	99.8%	99.6%
No. indep. Reflns	12159	21657
No. obsd reflns with ($I>2\sigma(I)$)	9178	19177
No. refined params	509	563
GooF (F^2)	1.037	1.350
R_1 (F) ($I > 2\sigma(I)$)	0.0444	0.0504
wR_2 (F^2) (all data)	0.1149	0.1272
Largest diff peak/hole, e Å^{-3}	0.648 / –0.432	1.231/ –2.446
CCDC number	1914203	1914204

3. Computational Methodology.

Starting from the solid-state molecular geometries of **1** and **2** density functional theory (DFT) computations were performed in the gas-phase at the B3PW91/6-311+G(2df,p)[17] level of theory using Gaussian09.[S8] For the Rh atom, an effective core potential (ECP28MDF)[18] and corresponding cc-pVTZ basis set[18] were utilized. Dispersion effects were modeled using Grimme's GD3BJ parameters.[24] Subsequent normal mode analysis proved all structures to be local minima on the potential energy hypersurface. The resulting IR frequencies were scaled with a basis-set dependent factor of 0.9679 as obtained from reference [S9]. The wavefunction files were used for a topological analysis of the electron density according to the Atoms-In-Molecules space-partitioning scheme[19] using AIM2000,[S10] whereas DGRID[S11] was used to generate and analyze the Electron-Localizability-Indicator (ELI-D)[21] related real-space bonding descriptors[21] applying a grid step size of 0.05 a.u. (0.12 a.u. for visualization). The NCI[20] grids were computed with NCIplot (0.1 a.u. grids).[S12] Bond paths are displayed with AIM2000, while ELI-D and NCI figures are displayed with MolIso.[S13] The determination of the compliance constants and compliance coupling constants were carried out with the COMPLIANCE software (version 3.0.2)[22, S14] using the respective Gaussian *.log file containing the frequency analysis and are displayed with VMD.[S15] AIM provides a bond paths motif, which resembles and exceeds the Lewis picture of chemical bonding, disclosing all types and strengths of interactions. Additionally, it provides atomic volumes and charges. Analyses of the reduced density gradient, $s(\mathbf{r}) = [1/2(3\pi^2)^{1/3}]|\nabla\rho|/\rho^{4/3}$, according to the NCI method is used to visualize non-covalent bonding aspects. An estimation of different non-covalent contact types according to steric/repulsive ($\lambda_2 > 0$), van der Waals-like ($\lambda_2 \approx 0$), and attractive ($\lambda_2 < 0$) is facilitated by mapping the ED times the sign of the second eigenvalue of the Hessian ($\text{sign}(\lambda_2)\rho$) on the *iso*-surfaces of $s(\mathbf{r})$. AIM and NCI are complemented by the ELI-D, which provides electron populations and volumes of bonding

and lone-pair basins and is especially suitable for the analysis of (polar-)covalent bonding aspects.

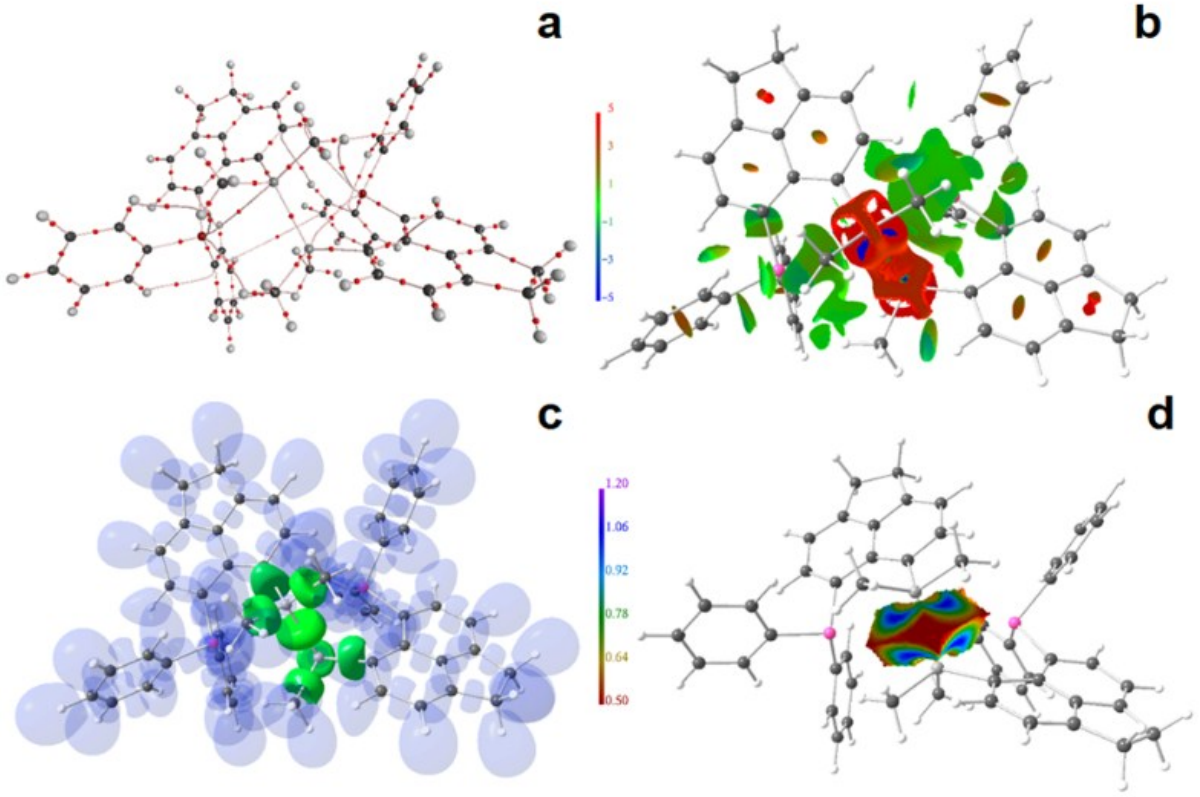

Figure S5. RSBI analysis of **1**. (a) AIM bond paths motif, (b) NCI *iso*-surface at s(r) = 0.5, (c) ELI-D localization domain representation at *iso*-value of 1.3, (d) ELI-D distribution mapped on a Si-Si ELI-D basin.

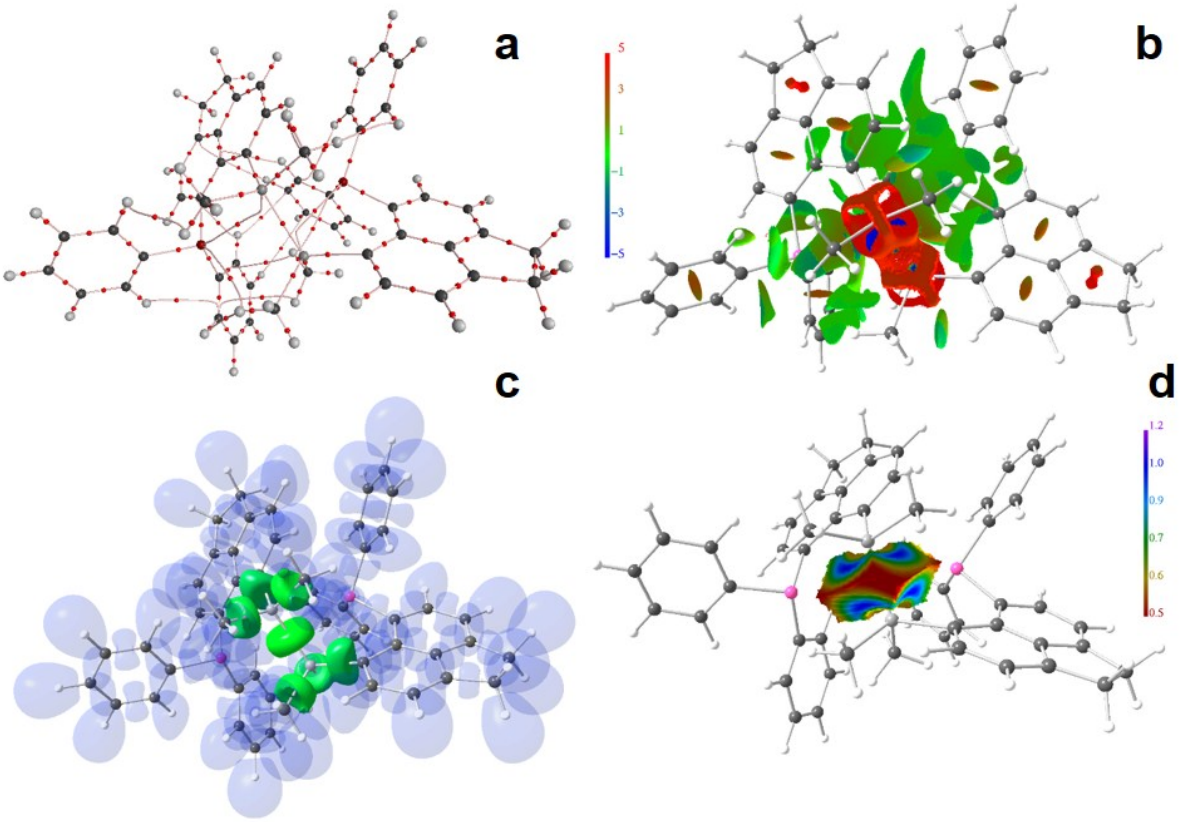

Figure S6. RSBI analysis of **1** with the inclusion of empirical dispersion. (a) AIM bond paths motif, (b) NCI *iso*-surface at s(r) = 0.5, (c) ELI-D localization domain representation at *iso*-value of 1.3, (d) ELI-D distribution mapped on a Si-Si ELI-D basin.

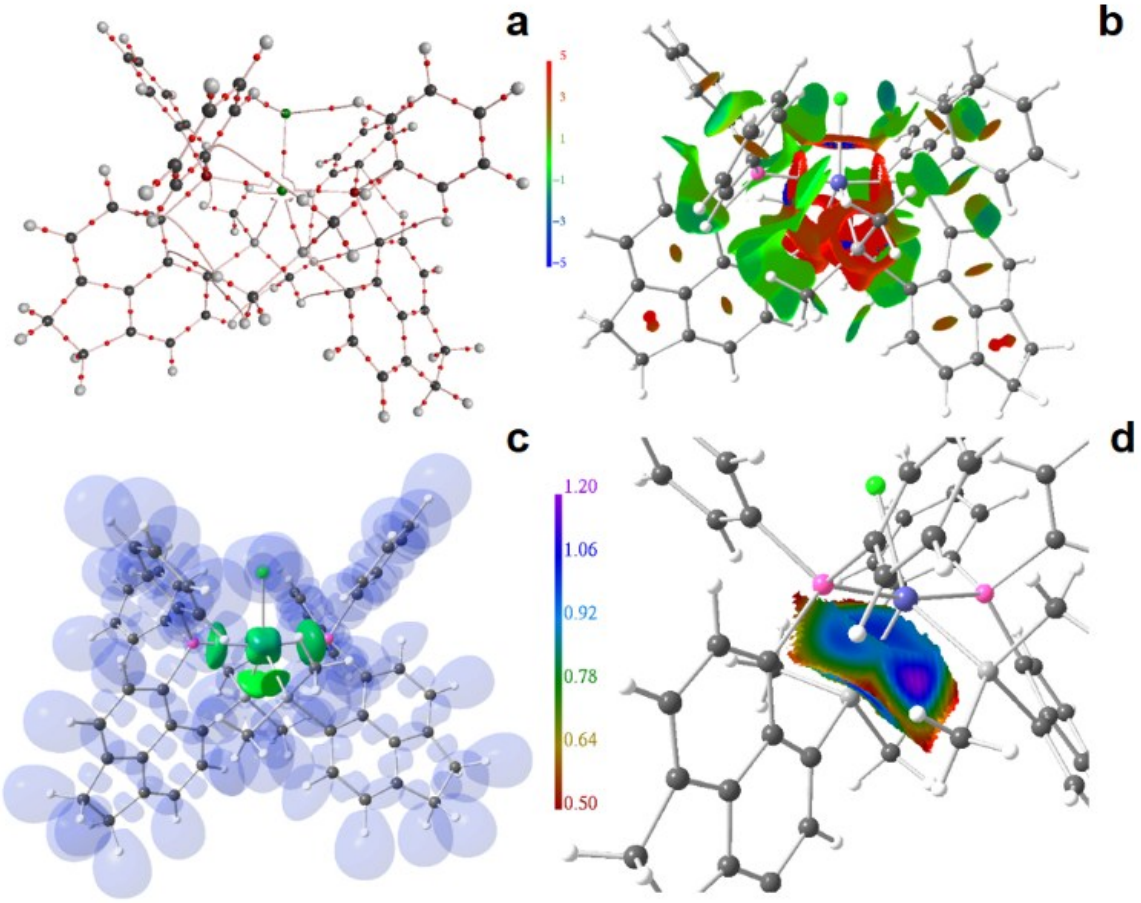

Figure S7. RSBI analysis of complex **2**. (a) AIM bond paths motif, (b) NCI *iso*-surface at s(r) = 0.5, (c) ELI-D localization domain representation at *iso*-value of 1.3, (d) ELI-D distribution mapped on a Si-Si ELI-D basin.

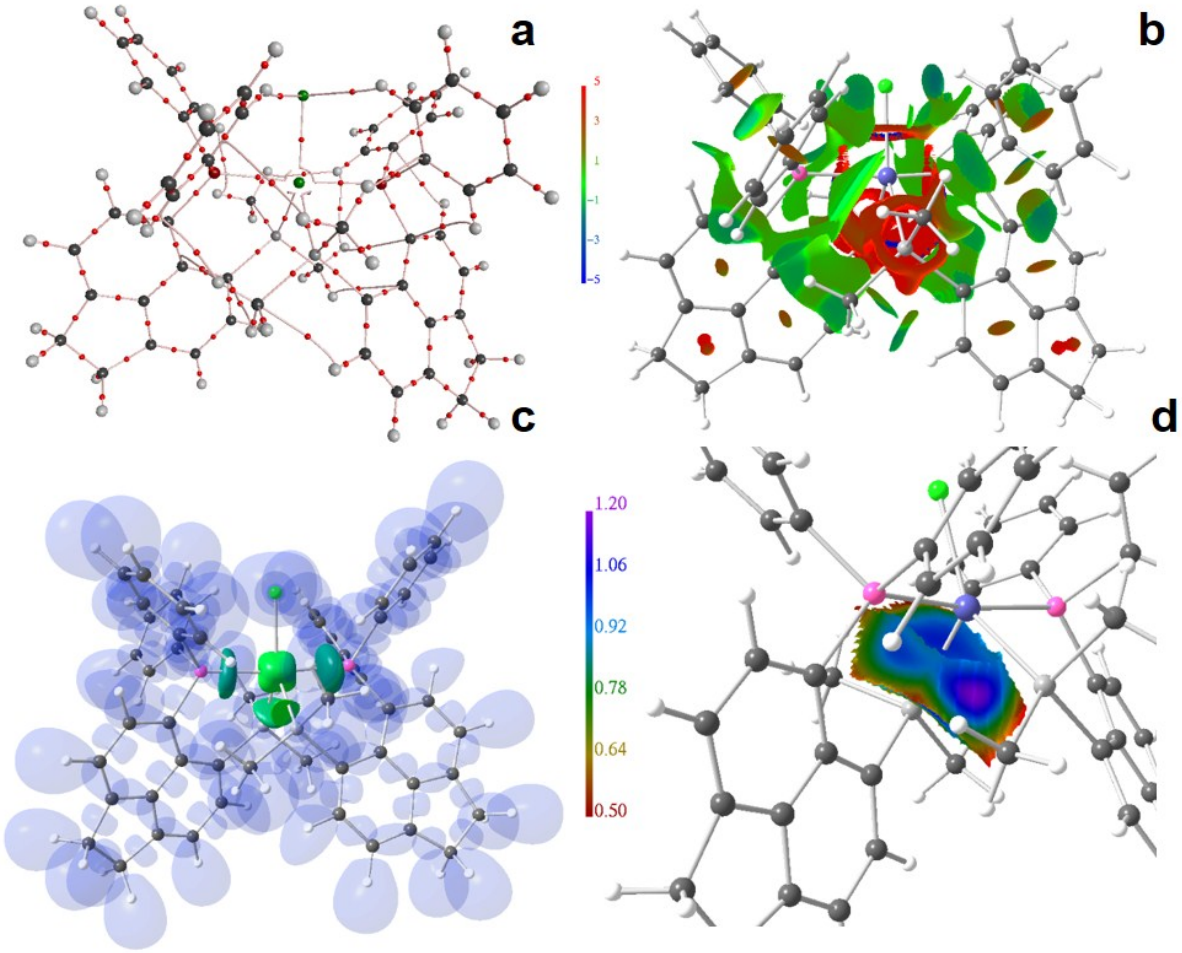

Figure S8. RSBI analysis of complex **2** with the inclusion of empirical dispersion. (a) AIM bond paths motif, (b) NCI *iso*-surface at s(r) = 0.5, (c) ELI-D localization domain representation at *iso*-value of 1.3, (d) ELI-D distribution mapped on a Si-Si ELI-D basin.

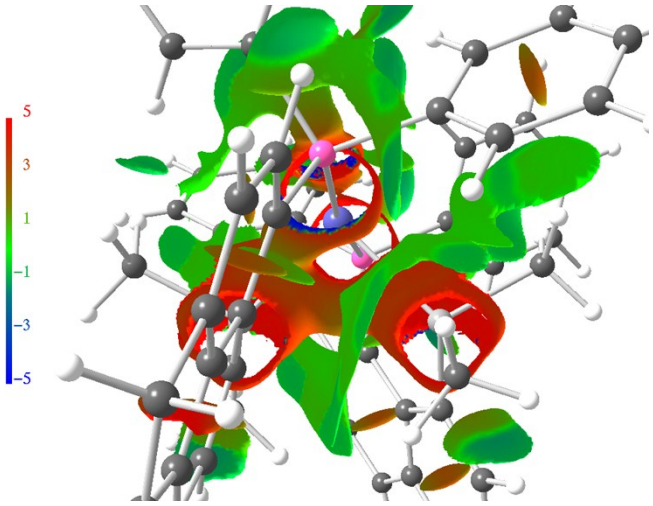

Figure S9. NCI *iso*-surface at s(**r**) = 0.5 of **2**. Side view.

Table S2. Topological and integrated bond properties from AIM and ELI-D. Values derived from the inclusion of empirical dispersion are given in italics.

	contact or basin	d [Å]	ρ(r) [eÅ-3]	$\nabla^2\rho(r)$ [eÅ^{-5}]	ε	G/ρ(r) [a.u.]	H/ρ(r) [a.u.]
1	Si-Si	2.393	0.60	–3.3	0.00	0.07	–0.45
		2.351	*0.64*	*–3.7*	*0.01*	*0.08*	*–0.48*
	Si1-P1	3.362	0.08	0.6	0.63	0.47	0.02
		3.272	*0.12*	*0.7*	*1.63*	*0.43*	*–0.04*
	Si2-P2	3.454	0.07	0.6	0.87	0.50	0.04
		3.309	*0.10*	*0.6*	*1.30*	*0.45*	*–0.02*
	Si-Me	1.898	0.80	2.6	0.03	0.92	–0.69
		1.893	*0.80*	*2.8*	*0.03*	*0.93*	*–0.69*
	Si-ace	1.924	0.75	2.9	0.08	0.93	–0.66
		1.909	*0.77*	*3.4*	*0.07*	*0.96*	*–0.66*
2	Rh-Si1	2.349	0.60	–2.4	0.04	0.30	–0.59
		2.329	*0.62*	*–2.6*	*0.03*	*0.32*	*–0.62*
	Rh-Si2	2.312	0.62	–2.4	0.07	0.38	–0.66
		2.279	*0.64*	*–2.0*	*0.07*	*0.47*	*–0.69*
	Rh-P1	2.343	0.64	2.8	0.05	0.69	–0.38
		2.292	*0.70*	*2.9*	*0.04*	*0.71*	*–0.42*
	Rh-P2	2.346	0.63	3.0	0.01	0.71	–0.38
		2.299	*0.68*	*3.1*	*0.03*	*0.73*	*–0.41*
	Rh-Cl	2.433	0.48	4.4	0.27	0.90	–0.26
		2.421	*0.49*	*4.5*	*0.25*	*0.91*	*–0.26*
	Si-Me	1.902	0.79	2.6	0.02	0.92	–0.69
		1.895	*0.80*	*2.8*	*0.02*	*0.93*	*–0.69*
	Si-ace	1.911	0.77	3.3	0.05	0.97	–0.67
		1.898	*0.79*	*3.8*	*0.05*	*1.00*	*–0.67*

	contact or basin	N_{ELI} [e]	V_{ELI} [Å^3]	γ_{ELI}
1	Si-Si	2.06	10.7	2.42
		2.07	*9.6*	*2.41*
	Si1-P1	2.05	12.3	2.48
		2.01	*10.2*	*2.31*
	Si2-P2	2.06	13.0	2.48
		2.05	*11.8*	*2.38*
	Si-Me	1.98	5.4	1.98
		1.98	*5.3*	*1.98*
	Si-ace	2.33	8.0	2.03
		2.32	*7.2*	*2.04*
2	Rh-Si1	1.66	7.2	1.45
		1.66	*6.7*	*1.44*
	Rh-Si2	1.62	6.9	1.40
		1.61	*6.4*	*1.38*
	Rh-P1	2.07	7.9	1.68
		2.09	*7.4*	*1.64*
	Rh-P2	2.09	8.1	1.72
		2.11	*7.7*	*1.69*
	Rh-Cl	7.68	33.9	1.64
		7.68	*36.3*	*1.65*
	Si-Me	1.98	5.4	1.98
		1.98	*5.3*	*1.98*
	Si-ace	2.32	7.2	2.05
		2.33	*7.1*	*2.05*

For all bonds, $\rho(\mathbf{r})_{bcp}$ is the electron density at the bond critical point, $\blacklozenge^2\rho(\mathbf{r})_{bcp}$ is the corresponding Laplacian, $G/\rho(\mathbf{r})_{bcp}$ and $H/\rho(\mathbf{r})_{bcp}$ are the kinetic and total energy density over $\rho(\mathbf{r})_{bcp}$ ratios, N_{ELI} and V_{ELI} are electron populations and volumes of related ELI-D basins, γ_{ELI} is the ELI-D value at the attractor position. For Si-Me and Si-ace, the bond properties are averaged.

Table S3. AIM atomic and fragmental charges (in e) of **1** and **2**.

fragment	**1**	**2**	Δ
ace1	–1.18	–1.18	0.00
a1phe1	–0.50	–0.43	–0.07
a1phe2	–0.49	–0.43	–0.06
a1Me1	–0.68	–0.68	–0.01
a1Me2	–0.70	–0.67	–0.03
ace2	–1.18	–1.18	0.00
a2phe1	–0.50	–0.42	–0.08
a2phe2	–0.50	–0.45	–0.05
a2Me1	–0.70	–0.70	0.00
a2Me2	–0.69	–0.67	–0.02
P1	1.50	1.62	–0.12
P2	1.48	1.58	–0.10
Si1	2.08	2.38	–0.30
Si2	2.05	2.48	–0.43
Cl		–0.64	0.64
Rh		–0.60	0.60
Σ	–0.02	0.02	–0.04

4. Additional references

[S1] T.G. Do, E. Hupf, S. Mebs, E. Lork, S. Grabowsky, J. Beckmann, *Z. Anorg. Allg. Chem.* 2013, **639**, 2233-2249.

[S2] E. Hupf, S. Mebs, E. Lork, J. Beckmann, *Organometallics.* 2015, **34**, 3873-3887.

[S3] D. Duvinage, P. Bottke, M. Wark, E. Lork, S. Mebs, J. Beckmann *Eur. J. Inorg. Chem.* 2019, **5**, 712-720.

[S4] Z. Li, K. Iida, Y. Tomisaka, T. Hirao, A. Nomoto, A. Ogawa, *Organometallics*, 2007, **26**, 1212-1216.

[S5] L. J. Farrugia. *J. Appl. Cryst*. 1999, **32**, 837-838.

[S6] G. M. Sheldrick, *Acta Cryst*. 2008, **A64**, 112-122.

[S7] K. Brandenburg, H. Putz DIAMOND V3.1d, Crystal Impact GbR, 2006.

[S8] M. J. Frisch, G. W. Trucks, H. B. Schlegel, G. E. Scuseria, M. A. Robb, J. R. Cheeseman, G. Scalmani, V. Barone, B. Mennucci, G. A. Petersson, et al. *Gaussian09*, revision D.01; Gaussian, Inc.: Wallingford, CT, 2010.

[S9] M. P. Andersson, P. Uvdal, *J. Phys. Chem. A* 2005, ***109***, 2937-2941.

[S10] F. Biegler-König, J. Schönbohm, D. Bayles, *J. Comput. Chem*. 2001, **22**, 545-559.

[S11] M. Kohout, *DGRID*-4.6 Radebeul, **2015**.

[S12] J. Contreras-García, E. Johnson, S. Keinan, R. Chaudret, J.-P. Piquemal, D. Beratan, W. Yang, *J. Chem. Theor. Comp.* 2011, **7**, 625-632.

[S13] C. B. Hübschle, P. Luger, *J. Appl. Crystallogr*. 2006, **39**, 901-904.

[S14] K. Brandhorst, J. Grunenberg, *Chem. Soc. Rev.* 2008, **37**, 1558-1567.

[S15] W. Humphrey, A. Dalke, K. Schulten, VMD - Visual Molecular Dynamics. *J. Mol. Graphics* 1996, **14**, 33-38.